Catalysis Today 347 (2020) 10–17

Contents lists available at ScienceDirect

Catalysis Today

journal homepage: www.elsevier.com/locate/cattod

From nano- to macro-engineering of ZSM-11 onto thin-felt stainless-steel-fiber: Steam-assisted crystallization synthesis and methanol-to-propylene performance

Jia Ding, Zhiqiang Zhang, Chao Meng, Guofeng Zhao*, Ye Liu, Yong Lu*

Shanghai Key Laboratory of Green Chemistry and Chemical Processes, School of Chemistry and Molecular Engineering, East China Normal University, Shanghai 200062, China

ARTICLE INFO

Keywords:
Structured catalyst
ZSM-11
Steam-assisted crystallization
Methanol-to-propylene

ABSTRACT

Thin-felt ZSM-11/stainless-steel(SS)-fiber composites are successfully prepared via a combined washcoating and steam-assisted crystallization (SAC) method. Pre-aging of synthesis sol at a lower temperature of 80 °C can facilitate the zeolite nucleation and subsequent SAC growth at 180 °C. Such synthesis approach realizes the flexible tuning of acidity via adjusting SiO_2/Al_2O_3 molar ratio in a wide range, including but not limited from 105 to 425. The as-synthesized ZSM-11/SS-fiber composites are employed as catalysts for the methanol-to-propylene reaction, and the promising thin-felt catalyst with SiO_2/Al_2O_3 molar ratio of 200 shows remarkable stability improvement in comparison with its powdered counterpart, due to enhanced zeolite utilization efficiency and heat/mass transfer by the microfibrous-structured design.

1. Introduction

Structured zeolites are composites prepared by coating zeolites with various topologies onto a variety of monolithic porous substrates, such as ceramic foam [1], cordierite honeycomb [2,3], SiC foam [4–7], porous α-Al_2O_3 [8,9], and structured metallic substrates [10–14], which are promisingly used in absorption, separation and catalysis. Particularly, some structured zeolite catalysts have been developed in the heterogeneous catalysis process due to their improved hydrodynamics, enhanced heat/mass transfer, large area to volume ratio and high zeolite utilization efficiency, which are central to the notion of promoting the reactor performance [3,11,15–18].

Accordingly, substantial research efforts have been dedicated to developing novel structured zeolite catalysts for strongly endo/exothermic reactions. For instance, ZSM-5 coated ceramic foam and stainless-steel tube catalysts were synthesized by washcoating method and applied in methanol-to-olefins (MTO) and catalytic cracking reactions [1,10,19]. In addition, some ZSM-5/SiC foam and ZSM-5/metal-fiber catalysts were also assembled by in-situ hydrothermal synthesis method, which showed intrinsic stability and selectivity improvements in comparison with the conventional zeolite pellets in the methanol-to-propylene (MTP) and MTO processes [7,15,20,21]. Also, directly hydrothermal synthesized MCM-22/SiC structured catalyst exhibited good catalytic performance in the methane dehydroaromatization reaction after Mo loading [22]. Up to now, more than two hundred zeolitic frameworks have been defined and announced by the International Zeolite Association (IZA), but only a few of them have been structured. Hence, developing new-type structured zeolites (new framework structure or new substrate) is of great importance for the expansion of structured zeolite family and the process intensification of more heat/mass-transfer limited reactions.

ZSM-11 zeolite (MEL-type) with crossing straight channels and a maximum pore size of 0.55 nm has received much attention because of its optimum performances as a solid acid and shape-selective catalyst in various industrial processes, such as methanol-to-hydrocarbons (MTH) [23–25], catalytic cracking [26], isomerization [27], and hydrocracking [28]. Even so, pioneering work so far has never been reported on the fabrication and catalytic application of structured ZSM-11 zeolite. The prerequisite of employing structured ZSM-11 in the above-mentioned reactions is developing a producible fabrication process, since the widespread application of structured zeolites catalysts is always retarded by their poor adhesion, low zeolite loading, high cost, difficulty in scaling up and environmental pollution, brought by the traditional washcoating and hydrothermal synthesis methods. In summary, two major challenges remain in the structured zeolite fabrication processes: (1) choosing a substrate with both larger void volume and outer surface, on which a higher zeolite loading can be easily obtained; (2) the necessity to develop a highly-efficient synthesis strategy. One

* Corresponding author.
E-mail addresses: gfzhao@chem.ecnu.edu.cn (G. Zhao), ylu@chem.ecnu.edu.cn (Y. Lu).

https://doi.org/10.1016/j.cattod.2018.02.058
Received 29 December 2017; Received in revised form 22 February 2018; Accepted 28 February 2018
Available online 01 March 2018
0920-5861/

example in this aspect is a recently-developed method coupling washcoating and dry-gel conversion for the engineering of ZSM-5 and Beta onto a three-dimensional (3D) sinter-locked stainless-steel-fibers (SS-fiber) [14,29–31], which provides an inspiration in rational design of other structured zeolites.

The recently highlighted MTH process is an alternative route in olefin production, which can adapt alternative carbon sources, such as coal, natural gas, and renewable biomass. In the previous works, it is confirmed that both the Beta/SS-fiber and ZSM-5/SS-fiber catalysts show marked catalytic performance improvement in MTH process as compared to their powdered counterparts [12,20,31,32], but the former with BEA-type structure gives a poor stability due to its larger pore size [31]. Actually, most of the acidic zeolite catalysts can convert methanol into hydrocarbons, such as ZSM-5 [33], ZSM-11 [34], SAPO-34 [35], Beta [36], MCM-22 [37] and SSZ-13 [38]. However, only ZSM-5 (used in MTP process with propylene as predominant product) and SAPO-34 (used in MTO process with light olefins as predominant product) have been put into large-scale application. Due to the combined unique pentasil structure (MFI-type) and microstructured design, all the ZSM-5/SS-fiber and alkali-treated hollow-ZSM-5/SS-fiber catalysts show promising MTP working-durability [14,29,30,39]. As another pentasil zeolite, ZSM-11 with MEL-type structure is also very stable in the MTP process, and even better than ZSM-5 sometimes [34], but to the best of our knowledge, ZSM-11 has not been structured yet. Hence, it is worthwhile to develop novel ZSM-11/SS-fiber catalyst and used for the MTP reaction.

Herein, a highly-efficient one-step “macro-meso-nano” synthesis is developed to in situ mount ZSM-11 layer onto SS-fiber substrate. After washcoating and drying, a uniform dry-gel layer containing structure-directing agent is formed along with the fibers and subsequently translated into zeolite ZSM-11 via steam-assisted crystallization (SAC) process. Such one-step synthesis strategy realizes the flexible tuning of acidity via adjusting the synthesis dry-gel SiO_2/Al_2O_3 molar ratio from 105 to 425, as well as the full use of raw materials with much less waste produced. More interestingly, the zeolite layer of as-synthesized ZSM-11/SS-fiber contains remarkable mesoporosity with high external surface area (e.g., 61 $m^2\ g_{zeolite}^{-1}$ and 0.10 $cm^3\ g_{zeolite}^{-1}$, not including the mass of SS-fibers). In the MTP reaction process, ZSM-11/SS-fiber catalyst shows a remarkable stability and selectivity improvement in comparison with the powdered ZSM-11 counterpart, which is in nature originated from the microfibrous-engineered design.

2. Experimental sections

2.1. Preparation of ZSM-11/SS-fiber

A sinter-locked microfibrous structure with entirely open 3D porous network, consisting of 15 vol% 316-L SS-fiber (20 μm in dia., Western Metal Material Co. Ltd., China) and 85 vol% voidage, was utilized as substrate. It was sonicated in acetone for 2 h, thoroughly washed by deionized water, and then dried at 100 °C overnight before used to avoid any contamination.

The typical procedure for the synthesis of ZSM-11/SS-fiber consists of two steps: placing the synthesis dry-gel onto the SS-fiber substrate and then translating such dry-gel coats into zeolite. The synthesis sol for washcoating was prepared as following: Firstly, a certain amount of sodium aluminate ($NaAlO_2$, C.P., Sinopharm Chemical Reagent Co., Ltd.) was dissolved in deionized water, and then tetrabutylammonium hydroxide (TBAOH, 25 wt% in water, Sinopec Co., Ltd.) was added under stirring, followed by the addition of silica sol (30 wt% SiO_2 in water). The obtained synthesis sol had a molar composition of $1SiO_2$: $(1/x)Al_2O_3$: yTBAOH: $60H_2O$, where “x” and “y” represent the SiO_2/Al_2O_3 and $TBAOH/SiO_2$ molar ratios. Such synthesis sol was pre-aged at 80 °C under stirring for 12 h before used. Then, circular chips of thin-felt SS-fibers (16.1 mm in dia.) were repeatedly dip-coated using synthesis sol and dried at 100 °C until to a desired amount of dry-gel.

Subsequently, in order to translate the dry-gel coats into ZSM-11, 40 circular chips (~10 g) of the resulting dry-gel/SS-fiber (dry-gel content of ~20 wt%) as well as 15 mL of water (H_2O/dry-gel mass ratio of ~7.5) were transferred into a 100 mL Teflon-lined stainless-steel autoclave, in which the composites were physically separated from water by a stainless-steel mesh. Crystallization was carried out at 180 °C, then the obtained product was dried at 100 °C, calcined at 550 °C for 5 h to remove the organic templates.

For acidic characterization and catalytic test, ZSM-11/SS-fiber composites were transformed into their H-form by ion-exchange with an aqueous solution of 1 mol L^{-1} NH_4Cl at 80 °C for 3 h and subsequently calcining at 550 °C for 5 h. The content of zeolite layer was estimated by the weight gain of the pristine microfibrous substrates after SAC synthesis.

2.2. Characterization

Powder X-ray diffraction (XRD) patterns were collected on a Rigaku Ultima IV desktop X-ray diffractometer with monochromated Cu Kα radiation (0.154 nm, 35 kV, and 25 mA). N_2 adsorption/desorption isotherms were measured at 77 K on a BEL-MAX gas adsorption analyzer. For the sole ZSM-11 layer, specific surface area (SSA) and pore volume were calculated via dividing the as-measured data of the ZSM-11/SS-fiber composite by the zeolite mass content. The actual chemical composition of ZSM-11/SS-fiber samples was determined by inductively coupled plasma atomic emission spectroscopy (ICP-AES, ICP Thermo IRIS Intrepid II XSP, USA). The layer surface morphology of ZSM-11/SS-fiber composites was characterized by the scanning electron microscopy (SEM, Hitachi S-4800, Japan). The transmission electron microscopy (TEM) images were obtained on a Tecnai G^2 F30 electron microscope. Temperature-programmed desorption of ammonia (NH_3-TPD) was performed on a Xianquan TP-5080 chemisorption analyzer. Thermogravimetric analysis (TGA) was conducted in flowing air (50 mL min^{-1}) on a Mettler Toledo TGA/DSC 3+ instrument at a heating rate of 10 °C min^{-1}, to determine the amount of coke deposit during the MTP reaction.

2.3. Catalytic evaluation

The obtained microfibrous-structured ZSM-11/SS-fiber composites were tested in the MTP reaction as described in detail elsewhere [20]. A fixed-bed quartz tube reactor (i.d., 16 mm; reactor length of 720 mm) was used for such reaction at 450 °C and methanol weight hourly space velocity (WHSV, to zeolite mass) of 5 h^{-1} under atmospheric pressure. Circular chips (16.1 mm diameter) of the ZSM-11/SS-fiber catalysts were packed layer-by-layer into the tube reactor. The zeolite mass in the microfibrous-structured catalysts was 0.4 g (not including the mass of SS-fiber). By using a high-performance liquid chromatography (HPLC) pump, anhydrous methanol (A.R., Sinopharm Chemical Reagent Co., Ltd.) was fed continuously, and followed by vaporization at 200 °C in highly purified N_2 flow to obtain a mixture feed with methanol concentration of 30 vol%. Effluent gas was quantitatively analyzed by an on-line Shimadzu 2014C gas chromatography-flame ionization detector (GC-FID) with a 30-m HP-PLOT/Q capillary column. Methanol conversion was calculated on the basis of reactor inlet and outlet concentrations. Selectivity to the hydrocarbons was defined as the molar ratio of carbon in the hydrocarbon formed versus the methanol converted. For comparison, the ZSM-11/SS-fiber (H-form) composites were crushed to destroy the robust monolithic structure, followed by ultrasonic treatment to facilitate the separation of ZSM-11 from the SS-fiber substrate. The resulting ZSM-11 was pressed and then crushed and sieved to 100–300 μm as the powdered catalyst for MTP test.

The MTP reaction kinetic evaluations over obtained microfibrous-structured ZSM-11/SS-fiber and powdered ZSM-11 catalysts were investigated by measuring the methanol conversion against the space

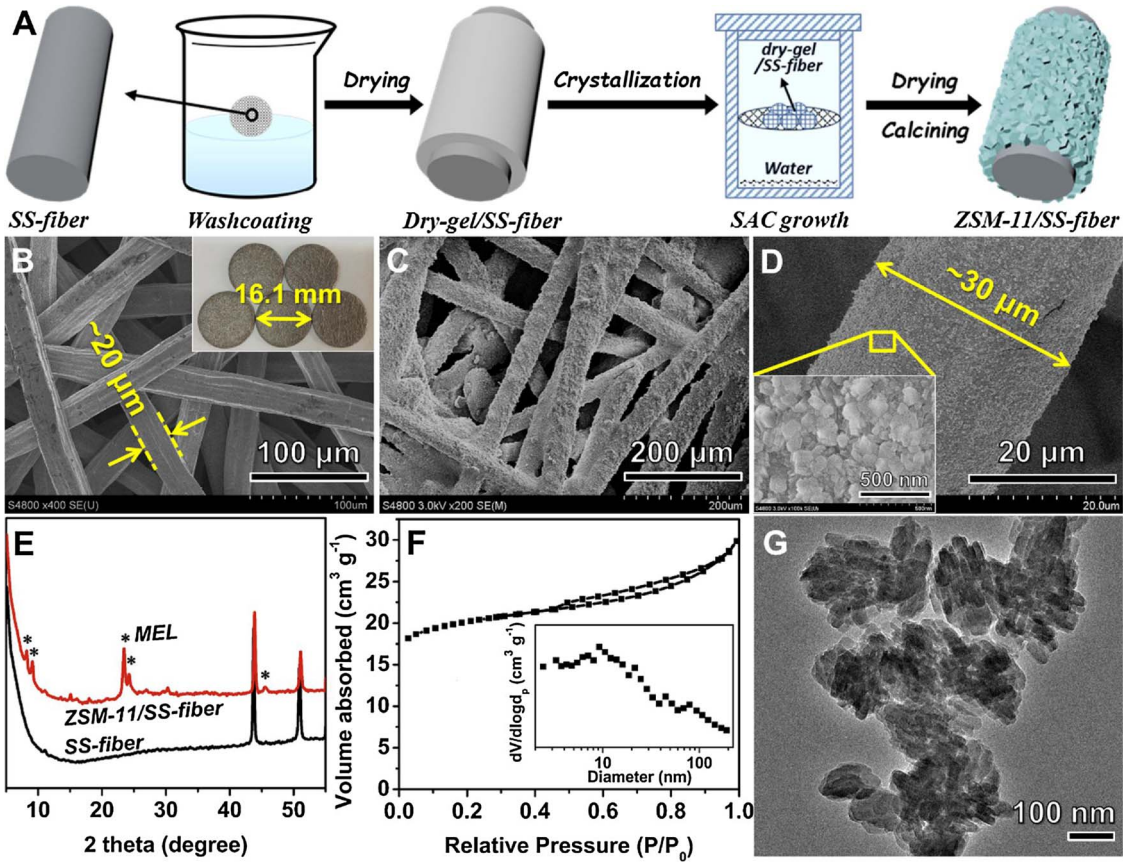

Fig. 1. (A) The schematic illustration for the fabrication strategy via combined washcoating and SAC method, (B) Photograph and SEM image of SS-fiber substrate, (C,D) SEM images, (E) XRD pattern, (F) N_2 adsorption-desorption isotherms and (inset) Barrett-Joyner-Halenda (BJH) mesopore size distribution (including the SS-fiber substrate) of the representative thin-felt ZSM-11/SS-fiber composite with a zeolite content of ~18.8 wt%, (G) TEM image of the zeolite layer in monolith.

time, as described in detail elsewhere [17]. At the beginning of the experiment, the reactor tube was heated in the highly purified N_2 flow (heating rate of 10 °C/min). For each test, the catalysts were packed into the reactor with a constant ZSM-11 zeolite mass of 0.2 g. Then, the flow of methanol and nitrogen was regulated according to a space time value of 32.0 $g_{zeolite}$ h/mol_{MeOH}, corresponding to the methanol WHSV (to zeolite mass) of 1 h^{-1}. The space time was gradually reduced (i.e., the WHSV was gradually increased) at intervals of 1 h by increasing the flow rate of gaseous mixture of 30 vol% methanol in N_2.

3. Results and discussion

3.1. Geometry, morphology and structural features of ZSM-11/SS-fiber

Fig. 1 shows the fabrication strategy as well as the geometry, morphology and structural/textural properties of the representative ZSM-11/SS-fiber composite (SiO_2/Al_2O_3 molar ratio of 200 by ICP-AES, TBAOH/SiO_2 of 0.2 and SAC time length of 48 h). Fig. 1A schematically illustrates the ZSM-11 zeolite engineered from macro- to nano-scale onto the thin-felt microfibrous SS-fiber substrate by a combined washcoating and SAC method. After multiplying the cycle of washcoating and drying, a dry-gel layer containing TBAOH is coated on the SS-fiber substrate (Fig. 1A and Fig. S1) to form a 3D porous dry-gel/SS-fiber monolith. Subsequently, the TBAOH-containing dry-gel layer is transformed into well-crystalline ZSM-11 at 180 °C for 48 h under water vapour (Fig. 1A–D). As shown in Fig. 1B–D, a uniform and dense zeolite layer is formed continuously along with the SS-fiber to form 3D-network ZSM-11/SS-fiber monolithic structure while macropores of the sinter-locked structure are well-preserved. The SEM image in Fig. 1D shows that the zeolite layer consists of abundant irregular particles with size of 100–200 nm. Due to the intergrowth of crystals, monolithic ZSM-11/SS-fiber composites have a high adherence of zeolite layer, showing weight loss of < 0.2 wt% after ultrasonic treatment in petroleum ether for 20 h [40].

The XRD patterns in Fig. 1E show that as-synthesized ZSM-11/SS-fiber monolith exhibits typical MEL structure with high crystallinity, as evidenced by the major XRD diffraction peaks located at the ranges of 2θ = 7–9° and 2θ = 22–25°, and no impurities phase is detected [41]. The N_2 adsorption-desorption isotherms of the ZSM-11/SS-fiber in Fig. 1F display a steep increase at very low relative pressure (P/P_0 < 0.1), indicating the well-constructed microporosity of ZSM-11 layer. Such monolithic composite with ~18.8 wt% ZSM-11 zeolite presents a total BET specific surface area (SSA) of 67.8 $m^2\,g^{-1}$ with a micropore volume of 0.027 $cm^3\,g^{-1}$ (including the mass of SS-fibers). Correspondingly, the pure ZSM-11 layer possesses a micropore SSA and volume of 300 $m^2\,g_{zeolite}{}^{-1}$ and 0.14 $cm^3\,g_{zeolite}{}^{-1}$ respectively, comparable to those of previously-reported ZSM-11 zeolites [24,26]. In addition, the appearance of a clear hysteresis loops at the relative pressure of 0.4-1.0 on isotherms suggests that the ZSM-11/SS-fiber composite has an appreciable mesoporous feature. For sole zeolite layer, the external SSA and mesopore volume are 61 $m^2\,g_{zeolite}{}^{-1}$ and 0.10 $cm^3\,g_{zeolite}{}^{-1}$ respectively. Barrett-Joyner-Halenda (BJH) pore size distribution curve in Fig. 1F shows that the mesopores of ZSM-11/SS-fiber composite have a board size distribution centered at ~9 nm. The TEM image in Fig. 1G reveals that the bulk crystals in zeolite layer consist of rod-like nanocrystals with diameter of ~20 nm, and abundant intercrystalline mesopores are observed among the nano-rods. These results indicate the ZSM-11/SS-fiber composite has a hierarchical porous structure.

3.2. Effects of SAC conditions on the synthesis of ZSM-11/SS-fiber

The ZSM-11/SS-fiber composites with different TBAOH amount used were synthesized at 180 °C for 48 h with a SiO_2/Al_2O_3 molar ratio of 200 in the synthesis sol. As the XRD patterns shown in Fig. S2, it is found that the dry-gel containing a low content of TBAOH (TBAOH/SiO_2 molar ratio of 0.05) is hardly converted into zeolite ZSM-11 through our SAC process. Yu and coworkers reported that a low TBAOH/SiO_2 molar ratio of 0.01 in synthesis precursor was capable of inducing high-crystalline ZSM-11 [42]. However, in order to gain a synthesis sol with suitable viscosity for washcoating, the use of mineralizer (such as NaOH) is deliberately avoided in our synthesis process. As a result, more TBAOH is needed to provide a very basic condition for the conversion of oxide forms of silicon and aluminum to useful precursors in tetrahedral coordination [43]. Indeed, as the TBAOH/SiO_2 molar ratio is increased from 0.05 to 0.1, intensified diffraction peaks of MEL structure are observed. However, the double-peak at 2θ = 45–46° suggests the obtained ZSM-11 layer is companied with some ZSM-5 fragments [44]. Further increasing the TBAOH/SiO_2 molar ratio to 0.2 or 0.3, zeolite layers in the monolithic composites show pure MEL phase. Hence, an appropriate TBAOH/SiO_2 molar ratio of 0.2 is used for further study.

Zeolite crystallization is a two-step process, including nucleation and crystal growth [45]. It is commonly known that pre-treatment may have significant impacts on the homogenization and nucleation of synthesis precursor, and thus the zeolite crystallization [46,47]. So, the promotion effect of pre-aging of synthesis sol on the formation of ZSM-11 layer is examined. Fig. 2A shows the XRD patterns of the ZSM-11/SS-fiber composites against the SAC time length, using a synthesis sol after pre-aged at 80 °C for 12 h. After a SAC for 3 h, the amorphous aluminosilicate dry-gel layer mounted onto the SS-fiber has already been translated into ZSM-11 zeolite with high crystalinity. The synthesis sol without pre-aging is also used directly for the preparation of ZSM-11/SS-fiber composites. As we can see from Fig. 2B, the dry-gel layer mounted on the SS-fiber using such unaged sol as coating sol remains almost unchanged until to 12 h SAC treatment, while clear ZSM-11 phase appears after a long SAC time length of 24 h. By comparison, it is undoubted that the synthesis sol pre-aging treatment facilitates the formation of ZSM-11 layer.

In addition, the zeolite crystallization process can be promoted by seed-assisted synthesis. As 5 wt% (in dry base) silicalite-2 seeding gel (containing pure-silica MEL-type seeds; Supporting Information for the preparation details; [48,49]) is added into the unaged synthesis sol, induction period is indeed shortened greatly (Fig. 2C). Generally, the seeds added into the synthesis gel can provide nucleation surface or act as “nuclei” directly, which would quicken the initial nucleation process [23,50,51]. This is the main cause for the fast crystallization of dry-gel derived from seed-containing synthesis sol (unaged), showing a crystallization curve in initial period (0–3 h) almost coincident with that of the ZSM-11/SS-fiber synthesized by using pre-aged sol (Fig. 2D). The above results in turn indicate that the aging process of the synthesis sol for coating is paramount for generating large amount of nuclei, which play the zeolite-seed-like roles in quickly consuming aluminosilicate precursors surrounding them to form ZSM-11 in the subsequent high-temperature SAC stage [52].

Fig. S3 shows the SAC time length dependent surface morphology evolution of the aluminosilicate dry-gel layer (coating by using the pre-aged synthesis sol with SiO_2/Al_2O_3 of 200 and TBAOH/SiO_2 of 0.2) in the ZSM-11/SS-fiber composites, monitored by means of SEM. Before SAC treatment (crystallization time length of 0 h), the dry-gel layer with smooth surface morphology is observed and uniformly mounted on the SS-fiber (Fig. S3A). After a SAC for only 3 h, numerous rod-like crystals are formed on the surface of dry-gel layer (Fig. S3B), corresponding to a higher relative ZSM-11 crystallinity of ~74% (Fig. 2D). With the increase in the SAC time length, the zeolite crystals become larger and angular (Fig. S3C–F). Especially, the rod-like stacks are changed to well-crystalline nano-crystals aggregates after a SAC for 48 h (Fig. 1D and Fig. S3F). As shown in Fig. 2D, the relative crystallinity of the zeolite

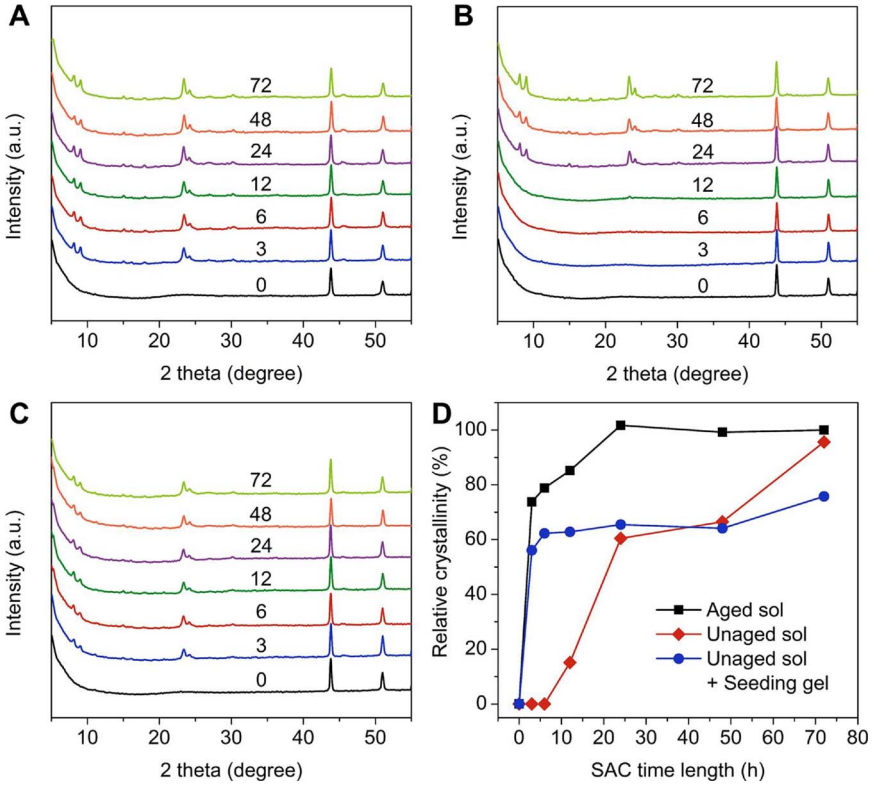

Fig. 2. XRD patterns of the ZSM-11/SS-fiber composites with various SAC time lengths synthesized by using (A) aged synthesis sol, (B) unaged synthesis sol as well as (C) unaged synthesis sol with silicalite-2 seeding gel, and (D) their corresponding crystallization curves based on the XRD analysis.

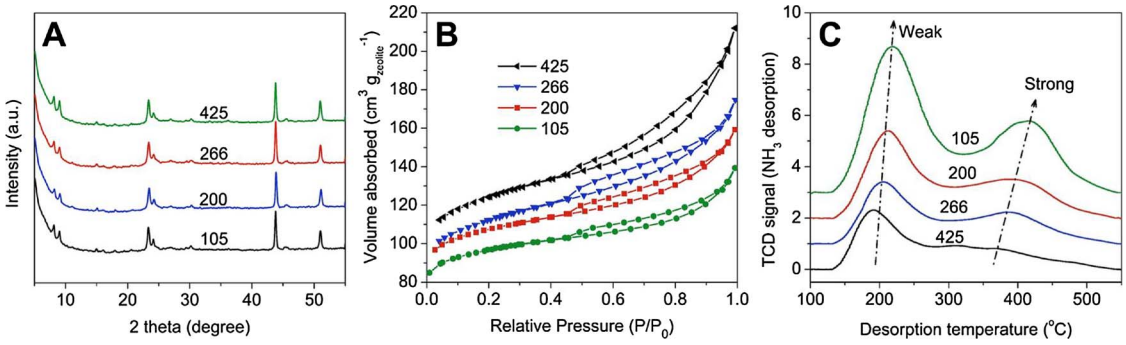

Fig. 3. (A) XRD patterns, (B) N_2 adsorption-desorption isotherms (not including the SS-fiber) and (C) NH_3-TPD profiles of the ZSM-11/SS-fiber composites with various SiO_2/Al_2O_3 molar ratios. Note: zeolite mass of 100 mg is used for the NH_3-TPD measurements.

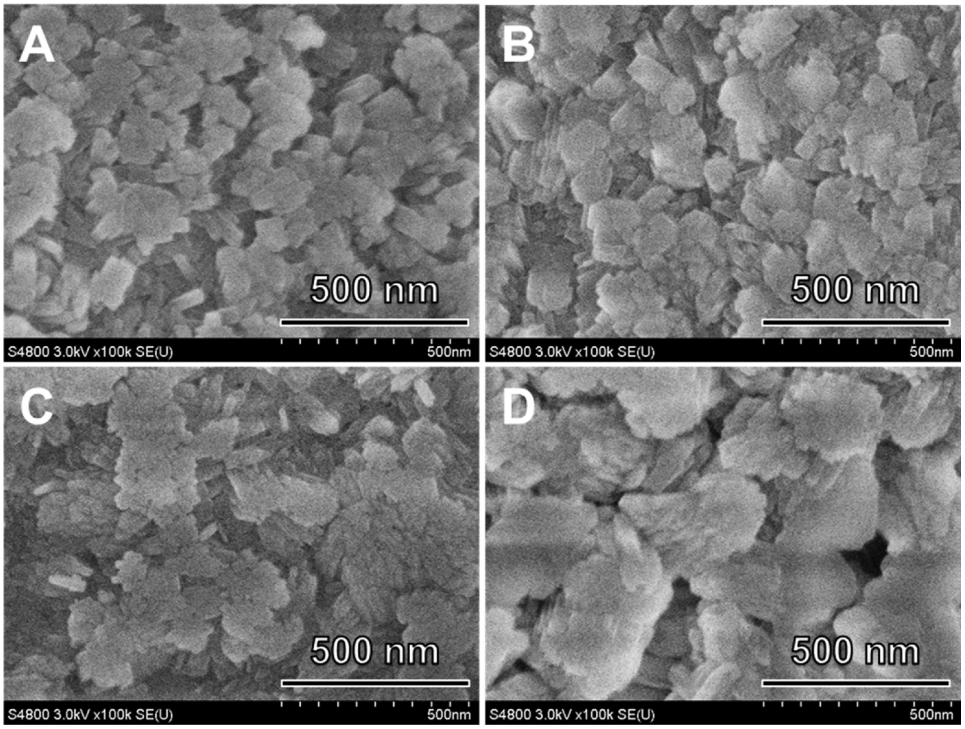

Fig. 4. SEM images of the ZSM-11/SS-fiber composites with different zeolite SiO_2/Al_2O_3 molar ratios of (A) 105, (B) 200, (C) 266 and (D) 425.

Table 1
Textural and acidic properties of zeolite layer in the microstructured ZSM-11/SS-fiber with various SiO_2/Al_2O_3 molar ratios.

Sample	S_{BET}[a] ($m^2\ g_{zeolite}^{-1}$)	S_{ext}[b] ($m^2\ g_{zeolite}^{-1}$)	V_{micro}[c] ($cm^3\ g_{zeolite}^{-1}$)	V_{meso}[d] ($cm^3\ g_{zeolite}^{-1}$)	V_{total}[e] ($cm^3\ g_{zeolite}^{-1}$)	Acidity[f] ($\mu mol\ g_{zeolite}^{-1}$)		
						Strong	Weak	Total
ZSM-11/SS-fiber-105	335	47	0.13	0.08	0.21	172	282	454
ZSM-11/SS-fiber-200	361	61	0.14	0.10	0.24	110	158	268
ZSM-11/SS-fiber-266	377	89	0.14	0.13	0.27	88	112	200
ZSM-11/SS-fiber-425	418	93	0.15	0.17	0.32	72	99	171

[a] N_2-BET specific surface area determined by Brunauer-Emmett-Teller method.
[b] External specific surface area determined by the t-plot method.
[c] Micropore volume determined by t-plot method.
[d] Mesopore volume; $V_{meso} = V_{total} - V_{micro}$.
[e] Total pore volume at $p/p_0 = 0.99$.
[f] The quantities of weak and strong acid sites determined by NH_3-TPD.

layer in the ZSM-11/SS-fiber samples is no longer altered significantly after the SAC for 24 h.

Fig. S4 provides the N_2 adsorption-desorption isotherms of sole aluminosilicate layer of the ZSM-11/SS-fiber samples in different SAC stages (not including the SS-fiber substrate). Clearly, the sole dry-gel (being calcined at 550 °C for 5 h; before undergoing SAC treatment) shows a type-IV curve without uptake at low relative pressure (Fig. S4A), indicating the absence of microporosity; a large H_2-type hysteresis loop is observed at the relative pressure range of $P/P_0 = 0.4–0.8$, in accordance with the obvious mesopores distributed at ca. 3.7 nm as the

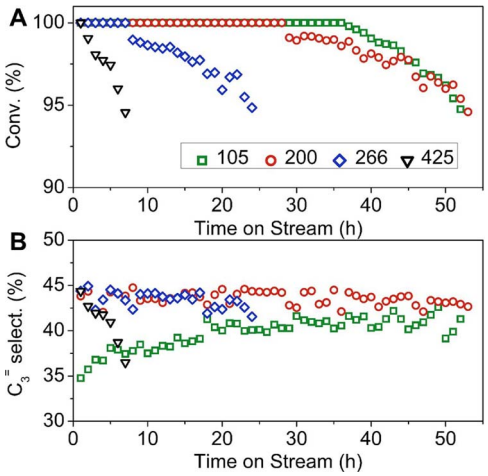

Fig. 5. (A) Methanol conversion and (B) C_3 = selectivity against the time on stream of ZSM-11/SS-fiber composites (SAC time length of 48 h) with various SiO_2/Al_2O_3 molar ratios in the MTP process. Reaction conditions: 450 °C, $WHSV_{MeOH}$ of 5 h^{-1}, 0.1 MPa, 30 vol% methanol in N_2, zeolite dosage of 0.4 g. Reaction is stopped at ~95% methanol conversion for quick screening.

result of the aggregation of amorphous particles (Fig. S4B). As can be seen from the calculated results listed in Table S1, the amorphous aluminosilicate dry-gel own has a N_2-BET SSA and total pore volume of 227 $m^2\ g_{zeolite}^{-1}$ and 0.20 $cm^3\ g_{zeolite}^{-1}$ (not including the mass of SS-fiber). A steep increase at low relative pressure ($P/P_0 < 0.1$) can be seen only after a SAC process for at least 3 h, in association with the observation of the decrease in the size of hysteresis loop, suggesting the mesoporosity is partly atrophied with the formation of zeolitic structure. With further prolonging the SAC treatment time length, the hysteresis loop shape and size remain almost unchanged whereas some mesopores fuse together to become larger ones (Fig. S4). As a result, the external SSA of zeolite layer is decreased from 95 to 68 $m^2\ g_{zeolite}^{-1}$ with a fixed mesopore volume of ~0.11 $cm^3\ g_{zeolite}^{-1}$. After a SAC for 24 h or longer, well-crystalized ZSM-11 layer is achieved with a high micopore volume of ~0.14 $cm^3\ g_{zeolite}^{-1}$.

The ZSM-11/SS-fiber composites can be synthesized with tunable SiO_2/Al_2O_3 molar ratio in a wide range from 105 to 425 (determined by ICP-AES), by adjusting the synthesis sol composition. The XRD patterns in Fig. 3A show that all the composites are featured of the MEL structure with almost equivalent characteristic peak intensity. Interestingly, the ZSM-11/SS-fiber composites show distinctive difference in their morphology (SEM images in Fig. 4). The ZSM-11 crystals enlarge with the increase in the SiO_2/Al_2O_3 molar ratio from 105 to 425. As previously noted [23,53], the apparent activation energies for pentasil zeolite (MFI and MEL) nucleation as well as crystal growth are much lower in the aluminum-free cases than in the aluminum-containing system. We thus speculate that ZSM-11 growth is favorable to form large crystals in case using a synthesis precursor with high SiO_2/Al_2O_3 molar ratio thereby leading to a slight increase in the micropore volume (Table 1 and Fig. 3B). The acidic properties of the ZSM-11/SS-fiber (H-form) composites with diverse zeolite SiO_2/Al_2O_3 molar ratios are characterized by means of NH_3-TPD, with the results as shown in Fig. 3C and Table 1. Clearly, the NH_3 desorption temperature for both weak (peaks centered at 190–220 °C) and strong (peaks centered at 370–420 °C) acid sites shows downward trend with the increase in the SiO_2/Al_2O_3 molar ratio, whereas the area of desorption peaks for either weak or strong acid sites shows opposite trend. This observation indicates that the low Si/Al ratio ZSM-11 structured onto the SS-fiber achieves high acid amount and strength, which is a generally acknowledged rule for ZSM-5 zeolite (both ZSM-11 and ZSM-5 are pentasil zeolites) [21,54–56].

3.3. Catalytic performance for MTP reaction

The ZSM-11/SS-fiber composites, with varied SiO_2/Al_2O_3 molar ratios, were examined in the recently highlighted zeolitic acid-catalyzed MTP process, at 450 °C using a high WHSV of 5 h^{-1} (for quick screening) for a feed gas of 30 vol% methanol in N_2. As shown in Fig. 5, the ZSM-11/SS-fiber-200 (SiO_2/Al_2O_3 molar ratio of 200 by ICP-AES) is the most stable catalyst, delivering a single-run lifetime of 52 h (time till to a methanol conversion less than 95%). Notably, the ZSM-11/SS-fiber-200 also achieves a high propylene selectivity of 44.3% and a total light olefins ($C_{2\text{-}4}^=$) selectivity of 67.2% (Table 2). The propylene selectivity as well as the single-run lifetime shows a volcano-shaped evolution behavior against the zeolite SiO_2/Al_2O_3 molar ratio from 105 to 425 whereas the total light olefins selectivity shows a monotonous downward trend but the P/E ratio ($C_3^=/C_2^=$) a monotonous upward trend (Table 2 and Fig. 5). It is not surprising because, as well noted previously [20,21,56], the relatively strong acid strength together with relatively high acid density is unfavorable for the propylene formation as well as the catalyst lifetime in the zeolite-catalyzed MTP process, due to the increased possibility of occurrence of the bimolecular hydrogen transfer reactions that favor coke formation [57–59]. For instance, the ZSM-11/SS-fiber-105 (SiO_2/Al_2O_3 ratio: 105, by ICP-AES) achieves a single-run lifetime of 51 h slightly shorter than that (52 h) for the ZSM-11/SS-fiber-200 (SiO_2/Al_2O_3 ratio: 200, by ICP-AES), delivering remarkably low propylene selectivity of 38.1% compared to that of 44.3% over the latter. It should be noted that, on the other hand, relatively high SiO_2/Al_2O_3 ratio (> 200) not only lowers the target product selectivity but also dramatically quickens the catalyst deactivation (Table 2 and Fig. 5). In addition, high SiO_2/Al_2O_3 ratio is normally associated with the large crystal size (Fig. 4), which is also unfavorable for intracrystalline diffusion so as to bring about fast deactivation.

To highlight the beneficial properties from our microfibrous-structured design, the powdered (100–300 μm) and particulate (400–600 μm) ZSM-11 counterparts taken from the ZSM-11/SS-fiber-200 composite directly was also tested in the MTP reaction. As shown in

Table 2
MTP reaction catalyzed by the microstructured ZSM-11/SS-fiber and powdered ZSM-11 with various SiO_2/Al_2O_3 molar ratios.[a]

Sample	Conv. (%)	Select.[b] (%)									P/E[c]
		CH_4	C_2H_4	C_2H_6	C_3H_6	C_3H_8	C_4H_8	C_4H_{10}	C_5^+	$C_2^= \sim C_4^=$	
ZSM-11/SS-fiber-105	100	0.8	11.5	0.2	38.1	2.2	18.4	9.4	19.4	68.0	2.2
ZSM-11/SS-fiber-200	100	1.1	8.0	0.2	44.3	0.6	14.9	9.8	21.1	67.2	3.7
ZSM-11/SS-fiber-266	100	1.4	6.8	0.2	44.5	0.4	13.5	9.6	23.6	64.8	4.4
ZSM-11/SS-fiber-425	97.4	2.3	5.9	0.2	40.9	0.3	12.8	10.2	27.4	59.6	4.7
Powdered ZSM-11 (100–300 μm)[d]	97.9	1.5	9.5	0.2	43.9	0.5	11.5	9.3	23.6	64.9	3.1
Particulate ZSM-11 (400–600 μm)[d]	88.9	2.1	10.7	0.3	42.1	0.4	10.3	9.6	24.5	63.1	2.6

[a] Reaction conditions: WHSV (methanol weight flow rate to zeolite mass) = 5 h^{-1}, 0.1 MPa, zeolite 0.4 g.
[b] Data are collected in the 5th hour; calculation is on the basis of carbon.
[c] C_3H_6/C_2H_4 molar ratio.
[d] SiO_2/Al_2O_3 molar ratio of 200.

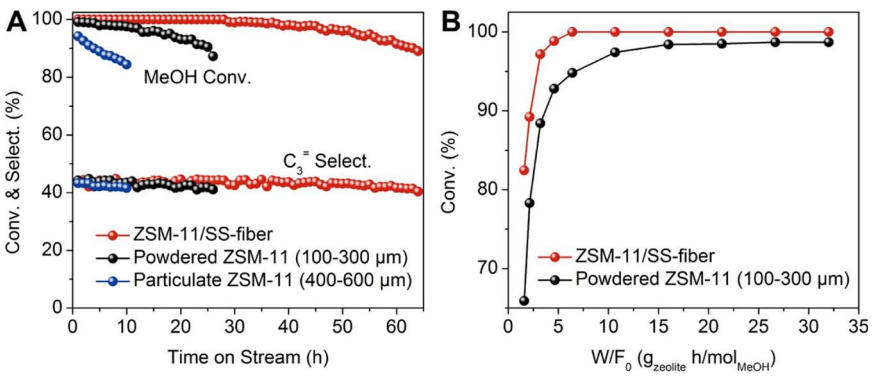

Fig. 6. (A) Methanol conversion with $C_3^=$ selectivity against the time on stream and (B) the methanol conversion against the space time of ZSM-11/SS-fiber, powdered ZSM-11 (100–300 μm) and particulate ZSM-11 (400–600 μm) in the MTP process (SiO_2/Al_2O_3 molar ratio of 200). Reaction conditions: (A) 450 °C, 0.1 MPa, 30 vol% methanol in N_2, zeolite dosage of 0.4 g, $WHSV_{MeOH}$ of 5 h^{-1}, and reaction is stopped at ~90% methanol conversion; (B) 450 °C, 0.1 MPa, 30 vol% methanol in N_2, zeolite dosage of 0.2 g.

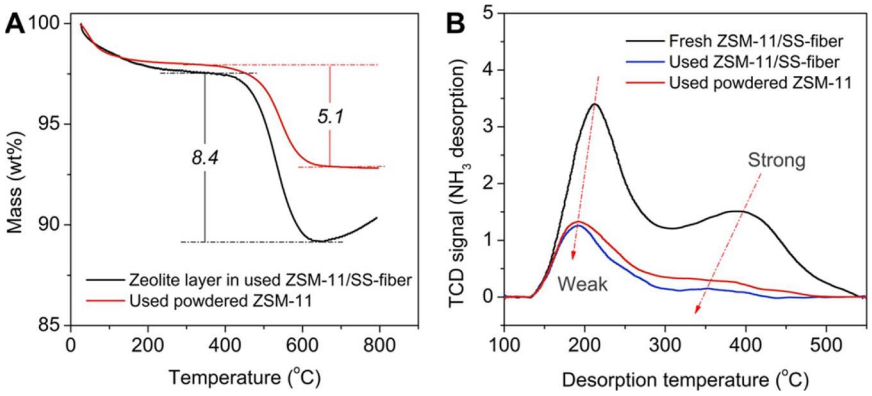

Fig. 7. (A) TGA profiles and (B) NH_3-TPD profiles of the spent catalyst samples (SiO_2/Al_2O_3 molar ratio of 200) after MTP reaction under the same reaction conditions as in Fig. 6A. Note: zeolite mass of 100 mg is used for NH_3-TPD measurements.

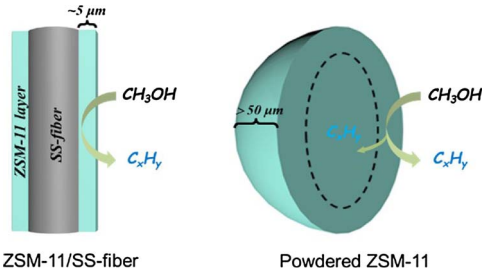

Fig. 8. Schematic illustration for MTP process over the ZSM-11/SS-fiber and powdered ZSM-11 (100–300 μm) respectively.

Fig. 6A, the powdered and particulate ZSM-11 counterpart catalysts fail to completely convert methanol initially. Not only that, our ZSM-11/SS-fiber-200 achieves a long lifetime of 63 h (at ~90% methanol conversion), about 1.5-fold longer than that (25 h) for the powdered ZSM-11 counterpart catalyst. Over the particulate ZSM-11 (400–600 μm) counterpart catalyst, methanol conversion dropped to ~90% within only 3 h. In addition, the powdered ZSM-11 counterpart catalyst delivers a $C_3^=$ selectivity of 43.9% associated with a $C_{2\text{-}4}^=$ selectivity of 64.9% in MTP process after 5 h on stream (Table 2), also lower than those (44.3% and 67.2%) of ZSM-11/SS-fiber-200 under identical reaction conditions.

To further understand the above-mentioned selectivity and stability improvements by microfibrous-structured design, a kinetic testing of MTP reaction was performed over both the ZSM-11/SS-fiber-200 and the powdered ZSM-11 (100–300 μm) counterpart catalyst. As shown in Fig. 6B, the ZSM-11/SS-fiber-200 catalyst is able to achieve complete methanol conversion until to a low space time less than 4.6 $g_{zeolite}$ h mol_{MeOH}^{-1}. In contrast, methanol cannot be fully converted over the powdered ZSM-11 counterpart catalyst even under a high space time of 32 $g_{zeolite}$ h mol_{MeOH}^{-1}; and accelerating descent inflection point of the methanol conversion comes at a relatively high space time of 10.7 $g_{zeolite}$ h mol_{MeOH}^{-1}, being 1.3 times higher than that (4.6 $g_{zeolite}$ h mol_{MeOH}^{-1}) for the microfibrous-structured composite. As noted in our previous report [17], the high inflection point of space time means the low utilization efficiency of zeolite acid sites because of their poor accessibility. Since the powdered ZSM-11 counterpart catalyst was directly obtained from the ZSM-11/SS-fiber-200 composites, pure zeolite parts in both of them should undoubtedly have equivalent acidic properties (strength and density). It is thus safe to say that our microfibrous-structured design makes the zeolite utilization efficiency doubled at least (tentatively estimated by their space time for inflection point of methanol conversion in Fig. 6B; i.e., 10.7/4.6).

The coke deposit amount on the used ZSM-11/SS-fiber-200 and powdered ZSM-11 catalysts (stopped at ~90% methanol conversion under WHSV of 5 h^{-1}) was measured using TGA method, with the results as shown in Fig. 7A. For the ZSM-11/SS-fiber-200 after 64 h reaction, the coke deposit amount in the zeolite is determined to be 8.4 wt% (not including the mass of SS-fiber), corresponding to an average coking rate of 1.3 mg $g_{zeolite}^{-1}$ h^{-1}. In contrast, the powdered ZSM-11 after 26 h reaction delivers a high coking rate of 2.0 mg $g_{zeolite}^{-1}$ h^{-1} whereas a low coke deposit amount is determined to be 5.1 wt%. These results indicate that the microstructured design facilitates the diffusion of coke precursors out of zeolite channels to form coke in the mesopores other than in the micropores [27,28], thereby leading to enhanced zeolite utilization with remarkable improvement of lifetime. The used ZSM-11/SS-fiber-200 and powdered ZSM-11 catalysts were further characterized by NH_3-TPD, showing marked decrease in both desorption temperature and peak area (Fig. 7B). Interestingly, the used ZSM-11/SS-fiber-200 loses near 95% of the strong acid sites whereas the used ZSM-11 powder catalyst shows a low loss of about 84% (Table S2), which in turn confirms the enhanced utilization of the acid sites by the microfibrous-structured design again, as schematically illustrated in Fig. 8.

4. Conclusions

The microfibrous-structured ZSM-11/SS-fiber composites are controllably synthesized by washcoating and subsequent SAC growth of zeolite layer on the SS-fiber substrates. It is found that a TBAOH/SiO_2 molar ratio of ≥0.2 is necessary for the growth of a pure ZSM-11 phase layer along with the SS-fiber. The synthesis sol pre-aging process at a low temperature of 80 °C can facilitate the zeolite nucleation and the subsequent SAC growth at 180 °C. The obtained ZSM-11/SS-fiber composites show well-developed mesoporosity derived from the aggregated mesopores in initial dry-gel. The ZSM-11/SS-fiber composites with controllable acid amounts are achievable via tuning the zeolite SiO_2/Al_2O_3 molar ratio from 105 to 425, which are examined in the MTP reaction and the most stable one is that with SiO_2/Al_2O_3 molar ratio of 200 in zeolite layer. Such optimized ZSM-11/SS-fiber composite also shows remarkable stability improvement as compared to its powdered counterpart because of enhanced zeolite utilization efficiency and mass transfer by the microfibrous-structured design.

Acknowledgements

This work was financially supported by the NSF of China (21773069, 21703069, 21473057, U1462129), and the “973 program” (2011CB201403) from the MOST of China.

Appendix A. Supplementary data

Supplementary data associated with this article can be found, in the online version, at https://doi.org/10.1016/j.cattod.2018.02.058.

References

[1] F.C. Patcas, J. Catal. 231 (2005) 194–200.
[2] B. Mitra, D. Kunzru, J. Am. Ceram. Soc. 91 (2007) 64–70.
[3] X. Huang, X.-G. Li, H. Li, W.-D. Xiao, Fuel Process. Technol. 159 (2017) 168–177.
[4] S. Ivanova, B. Louis, M.-J. Ledoux, C. Pham-Huu, J. Am. Chem. Soc. 129 (2007) 3383–3391.
[5] Y. Jiao, X. Fan, M. Perdjon, Z. Yang, J. Zhang, Appl. Catal. A 545 (2017) 104–112.
[6] X. Ou, S. Xu, J.M. Warnett, S.M. Holmes, A. Zaheer, A.A. Garforth, M.A. Williams, Y. Jiao, X. Fan, Chem. Eng. J. 312 (2017) 1–9.
[7] Y. Jiao, X. Yang, C. Jiang, C. Tian, Z. Yang, J. Zhang, J. Catal. 332 (2015) 70–76.
[8] L. Li, J. Yang, J. Li, J. Wang, J. Lu, D. Yin, Y. Zhang, AIChE J. 62 (2016) 2813–2824.
[9] Y. Tang, X. Liu, S. Nai, B. Zhang, Chem. Commun. 50 (2014) 8834–8837.
[10] Y. Cao, Y. Qiu, L. Wang, X. Zhang, G. Liu, J. Am. Ceram. Soc. 99 (2016) 2927–2936.
[11] L. Wang, Y. Wang, J. Hao, G. Liu, X. Ma, S. Hu, Appl. Catal. A 462–463 (2013) 271–277.
[12] X. Wang, M. Wen, C. Wang, J. Ding, Y. Sun, Y. Liu, Y. Lu, Chem. Commun. 50 (2014) 6343–6345.
[13] Q. Wen, J.C. Di, L. Jiang, J.H. Yu, R.R. Xu, Chem. Sci. 4 (2013) 591–595.
[14] J. Ding, Y. Jia, P. Chen, G. Zhao, Y. Liu, Y. Lu, Microporous Mesoporous Mater. 261 (2018) 1–8.
[15] S. Ivanova, B. Louis, B. Madani, J.P. Tessonnier, M.J. Ledoux, C. Pham-Huu, J. Phys. Chem. C 111 (2007) 4368–4374.
[16] Y. Jiao, C. Jiang, Z. Yang, J. Liu, J. Zhang, Microporous Mesoporous Mater. 181 (2013) 201–207.
[17] M. Wen, J. Ding, C. Wang, Y. Li, G. Zhao, Y. Liu, Y. Lu, Microporous Mesoporous Mater. 221 (2016) 187–196.
[18] J. Lefevere, S. Mullens, V. Meynen, J. Noyen, Chem. Papers 68 (2014).
[19] F. Meng, G. Liu, L. Wang, S. Qu, X. Zhang, Z. Mi, Energy Fuels 24 (2010) 2848–2856.
[20] M. Wen, X. Wang, L. Han, J. Ding, Y. Sun, Y. Liu, Y. Lu, Microporous Mesoporous Mater. 206 (2015) 8–16.
[21] J. Ding, L. Han, M. Wen, G. Zhao, Y. Liu, Y. Lu, Catal. Commun. 72 (2015) 156–160.
[22] L. Gu, D. Ma, G. Hu, J. Wu, H. Wang, C. Sun, S. Yao, W. Shen, X. Bao, Dalton Trans. 39 (2010) 9705–9710.
[23] Q. Yu, X. Tang, H. Yi, Chem. Eng. J. 314 (2017) 212–222.
[24] Z. Wei, K. Zhu, L. Xing, F. Yang, Y. Li, Y. Xu, X. Zhu, RSC Adv. 7 (2017) 24015–24021.
[25] X. Meng, Q. Yu, Y. Gao, Q. Zhang, C. Li, Q. Cui, Catal. Commun. 61 (2015) 67–71.
[26] W. Song, Z. Liu, L. Liu, A.L. Skov, N. Song, G. Xiong, K. Zhu, X. Zhou, RSC Adv. 5 (2015) 31195–31204.
[27] L. Zhang, H. Liu, X. Li, S. Xie, Y. Wang, W. Xin, S. Liu, L. Xu, Fuel Process. Technol. 91 (2010) 449–455.
[28] T.L.M. Maesen, M. Schenk, T.J.H. Vlugt, B. Smit, J. Catal. 203 (2001) 281–291.
[29] J. Ding, S. Fan, P. Chen, T. Deng, Y. Liu, Y. Lu, Catal. Sci. Technol. 7 (2017) 2087–2100.
[30] J. Ding, P. Chen, S. Fan, Z. Zhang, L. Han, G. Zhao, Y. Liu, Y. Lu, ACS Sustain. Chem. Eng. 5 (2017) 1840–1853.
[31] J. Ding, P. Chen, J. Zhu, G. Zhao, Y. Liu, Y. Lu, Microporous Mesoporous Mater. 250 (2017) 1–8.
[32] J. Ding, P. Chen, G. Zhao, Y. Liu, Y. Lu, J. Catal. 360 (2018) 40–50.
[33] J. Zhou, J. Teng, L. Ren, Y. Wang, Z. Liu, W. Liu, W. Yang, Z. Xie, J. Catal. 340 (2016) 166–176.
[34] F. Bleken, W. Skistad, K. Barbera, M. Kustova, S. Bordiga, P. Beato, K.P. Lillerud, S. Svelle, U. Olsbye, Phys. Chem. Chem. Phys. 13 (2011) 2539–2549.
[35] Z. Li, J. Martínez-Triguero, J. Yu, A. Corma, J. Catal. 329 (2015) 379–388.
[36] Z. Liu, X. Dong, Y. Zhu, A.-H. Emwas, D. Zhang, Q. Tian, Y. Han, ACS Catal. 5 (2015) 5837–5845.
[37] S. Wang, Z. Wei, Y. Chen, Z. Qin, H. Ma, M. Dong, W. Fan, J. Wang, ACS Catal. 5 (2015) 1131–1144.
[38] L. Wu, V. Degirmenci, P.C.M.M. Magusin, N.J.H.G.M. Lousberg, E.J.M. Hensen, J. Catal. 298 (2013) 27–40.
[39] J. Ding, Z. Zhang, L. Han, C. Wang, P. Chen, G. Zhao, Y. Liu, Y. Lu, RSC Adv. 6 (2016) 48387–48395.
[40] M. Valentini, G. Groppi, C. Cristiani, M. Levi, E. Tronconi, P. Forzatti, Catal. Today 69 (2001) 307–314.
[41] M.M.J. Treacy, J.B. Higgins, R. von Ballmoos, Zeolites 16 (1996) 323–802.
[42] Q. Yu, C. Li, X. Tang, H. Yi, Ind. Eng. Chem. Res. 54 (2015) 2120–2128.
[43] F. Pan, X. Lu, Q. Zhu, Z. Zhang, Y. Yan, T. Wang, S. Chen, J. Mater. Chem. A 2 (2014) 20667–20675.
[44] M. Conte, B. Xu, T.E. Davies, J.K. Bartley, A.F. Carley, S.H. Taylor, K. Khalid, G.J. Hutchings, Microporous Mesoporous Mater. 164 (2012) 207–213.
[45] G. Feng, P. Cheng, W. Yan, M. Boronat, X. Li, J.H. Su, J. Wang, Y. Li, A. Corma, R. Xu, J. Yu, Science 351 (2016) 1188–1191.
[46] Y. Zhu, Z. Hua, J. Zhou, L. Wang, J. Zhao, Y. Gong, W. Wu, M. Ruan, J. Shi, Chem. Eur. J. 17 (2011) 14618–14627.
[47] Q. Yu, C. Cui, Q. Zhang, J. Chen, Y. Li, J. Sun, C. Li, Q. Cui, C. Yang, H. Shan, J. Energy Chem. 22 (2013) 761–768.
[48] N. Kosinov, E.J.M. Hensen, J. Membr. Sci. 447 (2013) 12–18.
[49] S. Mintova, N. Petkov, K. Karaghiosoff, T. Bein, Microporous Mesoporous Mater. 50 (2001) 121–128.
[50] N. Ren, Z.-J. Yang, X.-C. Lv, J. Shi, Y.-H. Zhang, Y. Tang, Microporous Mesoporous Mater. 131 (2010) 103–114.
[51] C.S. Cundy, P.A. Cox, Microporous Mesoporous Mater. 82 (2005) 1–78.
[52] S. Gonthier, R.W. Thompson, Stud. Surf. Sci. Catal. 85 (1994) 43–73.
[53] A. Erdem, L.B. Sand, J. Catal. 60 (1979) 241–256.
[54] N.R. Meshram, S.G. Hegde, S.B. Kulkarni, Zeolites 6 (1986) 434–438.
[55] A.S. Al-Dughaither, H. de Lasa, Ind. Eng. Chem. Res. 53 (2014) 15303–15316.
[56] R. Wei, C. Li, C. Yang, H. Shan, J. Nat. Gas Chem. 20 (2011) 261–265.
[57] X. Sun, S. Mueller, Y. Liu, H. Shi, G.L. Haller, M. Sanchez-Sanchez, A.C. van Veen, J.A. Lercher, J. Catal. 317 (2014) 185–197.
[58] F. Ferreira Madeira, K. Ben Tayeb, L. Pinard, H. Vezin, S. Maury, N. Cadran, Appl. Catal. A 443–444 (2012) 171–180.
[59] L. Huang, P. Wang, J. Li, J. Wang, W. Fan, Microporous Mesoporous Mater. 223 (2016) 230–240.